

Double-strand DNA sensing Aim2 inflammasome regulates atherosclerotic plaque vulnerability

Paulin: Aim2 regulates atherosclerosis

Nicole Paulin, VetD^{1,2,3}, Joana R. Viola, PhD^{1,2}, Sanne L. Maas, MSc¹, Renske de Jong, MSc¹, Teresa Fernandes-Alnemri, PhD⁴, Christian Weber, MD^{1,2}, Maik Drechsler, PhD^{1,2*}, Yvonne Döring, PhD^{1,2*}, Oliver Soehnlein, MD, PhD^{1,2,5*}

* denotes equal contribution

¹ Institute for Cardiovascular Prevention (IPEK), LMU Munich, Munich, 80336, Germany.

² DZHK, partner site Munich Heart Alliance, Munich, 80336, Germany.

³ Centre for Preclinical Research, Klinikum Rechts der Isar, Munich, Germany.

⁴ Department of Biochemistry and Molecular Biology, Kimmel Cancer Center, Thomas Jefferson University, Philadelphia, Pennsylvania 19107, USA.

⁵ Department of Physiology and Pharmacology (FyFa), Karolinska Institutet, Stockholm, 17177, Sweden.

Contact information:

Oliver Soehnlein

Institute for Cardiovascular Prevention

Ludwig-Maximilians-University Munich

Pettenkoferstr. 9, 80336 Munich

Phone: +49-(0)89-4400-54667

Fax: +49-(0)89-4400-54352

Email: oliver.soehnlein@gmail.com

Word count: 1584

Main text word count: 796

Transparency and Openness Promotion (TOP) statement

The data, analytic methods, and study materials will be/have been made available to other researchers for purposes of reproducing the results or replicating the procedure. For requesting materials please contact the corresponding author.

Atherosclerosis, a lipid-driven sterile inflammatory disease of large arteries, and its sequelae such as myocardial infarction and stroke are the most frequent cause of death worldwide. While atherogenesis is characterized by the accumulation of inflammatory myeloid cells, destabilization of atherosclerotic lesions is dominated by necrotic core expansion and thinning of the fibrous cap. Sterile inflammation is typically induced by host-derived damage associated molecular patterns (DAMPs) which are sensed by pattern recognition receptors (PRRs). In recent years, cytosolic PRRs like the NLRP3 inflammasome have been connected to atherosclerosis as these can recognize (altered) self-structures such as lesional cholesterol crystals (1). Consequently, the inflammasome complex assembles promoting the release of pro-inflammatory cytokines IL1 β and IL18. The recent CANTOS trial lends strong support towards the importance of IL1 β in the context of atherosclerosis as therapeutic IL1 β neutralization in patients with established atherosclerotic disease, revealed a significant reduction in the incidence of a recurrent cardiovascular event (2).

Progression of atherosclerosis is characterized by the accumulation of dead cells. Several cell death pathways permitting release of nuclear double-stranded (ds)DNA have been identified including necrosis and NETosis. The amount of extracellular DNA correlates with the risk of cardiovascular events (3). Cytosolic dsDNA can be identified by Absent in melanoma 2 (Aim2) inflammasome leading to release of IL1 β and IL18 (4). Of note, Aim2 has recently been identified in human atherosclerotic lesions in proximity to necrotic cores (5). Here we study the inflammatory cascade upon dsDNA recognition in the context of atherosclerosis by genetically deleting or therapeutically inhibiting Aim2. All animal experiments were approved by the local ethics board.

We fed atherosclerosis-prone *Apoe*-deficient mice on a high cholesterol diet for 4 weeks or 4 months to model early and advanced stages of atherosclerosis, respectively. While staining for dsDNA at early stages was limited, larger quantities of dsDNA were found to accumulate extracellularly at advanced stages of atherosclerosis (**Figure A/B**). The primary sensor of dsDNA in the cytoplasm is Aim2 (4). In parallel with the heightened deposition of dsDNA during advanced atherosclerosis, we identified abundant Aim2 expression at later stages of atherosclerosis (**Figure C**). The expression of Aim2 was restricted to macrophages (**Figure D**), where dsDNA colocalized with Aim2 (**Figure E**).

To establish the role of Aim2 during atheroprogession, we compared lesion development in *Aim2*^{-/-}*Apoe*^{-/-} and littermate *Apoe*^{-/-} mice. After 4 weeks of high fat diet feeding, no differences in

lesion size, cellularity and macrophage content were found between the strains (not shown). In contrast, after 4 months on high fat diet (**Figure F-L**), intimal smooth muscle cells (SMCs) were strikingly increased in Aim2-deficient mice (**Figure G**), an observation paralleled by reduced TUNEL staining in these cells, increased lesional collagen content and thicker fibrous caps (**Figure H-J**). Together with a reduction in necrotic core area (**Figure K**), these findings are in agreement with an overall improvement of histopathological features of lesion stability in Aim2-deficient mice.

To study the therapeutic applicability of our findings we treated hypercholesterolemic mice with the Aim2-antagonizing synthetic oligonucleotide A151 or its vehicle during the last 8 weeks of a 4 months high fat diet feeding period (**Figure M-S**). Inhibition of Aim2 in this way led to a striking expansion of lesional SMC (**Figure N**). In line with observations made in Aim2-deficient mice, pharmacologic inhibition of Aim2 reduced SMC death, stimulated lesional collagen deposition, and permitted thickening of the fibrous cap (**Figure O-Q**). Together with reduced necrotic core sizes (**Figure R**), therapeutic inhibition of Aim2 reduced histopathological traits of lesion vulnerability. Of note, we were unable to detect differences in plasma cholesterol and triglyceride levels, in lesions sizes in the aortic roots and the aortic arch, as well as in lesional macrophage content in *ApoE*^{-/-} vs *Aim2*^{-/-} *ApoE*^{-/-} mice or in mice treated with PBS vs. A151 (not shown). In addition, deficiency of Aim2 or its inhibition reduced IL1 β and IL18 within atherosclerotic lesions (**Figure L/S**)

Here we report an important role of the dsDNA-Aim2 axis triggering a powerful cytokine response in lesional macrophages. Inhibition of Aim2 resulting in enhanced atherosclerotic lesion stability may reveal a promising new therapeutic concept in the treatment of atherosclerosis. The latter is strongly supported by data from the CANTOS trial showing that treatment with an IL1 β -blocking antibody decreases the risk of a recurrent cardiovascular event in patients with established atherosclerotic disease (2). However, treatment in this way also comes with heightened risk for infection, a side effect that may not be assumed by specific inhibition of Aim2. This notion is based on the understanding that Aim2 senses DAMPs accumulating in sterile inflammation; its inhibition may hence add a degree of selectivity towards the cause of the inflammation as compared to global inhibition of IL1 β and consequently be superior in elderly patients who not just suffer from cardiovascular disease but also having a compromised immune system.

Sources of funding

This study was supported by the German Research Foundation (SO876/6-1, SO876/11-1, SFB914 B08, SFB1123 A06 & B05), the Vetenskapsrådet (2017-01762), the Nederlandse Organisatie voor Wetenschappelijk Onderzoek (NOW) (VIDI project 91712303), the European Union's Horizon 2020 research and innovation programme under the Marie Skłodowska-Curie grant agreement No 675111, and the Förderprogramm für Forschung und Lehre (FöFoLe) program of the medical faculty of the Ludwig Maximilians University Munich.

Disclosure

None

List of references

1. Duewell P, Kono H, Rayner KJ, Sirois CM, Vladimer G, Bauernfeind FG, Abela GS, Franchi L, Nunez G, Schnurr M, Espevik T, Lien E, Fitzgerald KA, Rock KL, Moore KJ, Wright SD, Hornung V, Latz E. NLRP3 inflammasomes are required for atherogenesis and activated by cholesterol crystals. *Nature*. 2010;464:1357-1361. doi: 10.1038/nature08938.
2. Ridker PM, Everett BM, Thuren T, MacFadyen JG, Chang WH, Ballantyne C, Fonseca F, Nicolau J, Koenig W, Anker SD, Kastelein JJP, Cornel JH, Pais P, Pella D, Genest J, Cifkova R, Lorenzatti A, Forster T, Kobalava Z, Vida-Simiti L, Flather M, Shimokawa H, Ogawa H, Dellborg M, Rossi PRF, Troquay RPT, Libby P, Glynn RJ; CANTOS Trial Group. Antiinflammatory Therapy with Canakinumab for Atherosclerotic Disease. *N Engl J Med*. 2017;377:1119-1131. doi: 10.1056/NEJMoa1707914.
3. Borissoff JI, Joosen IA, Versteyleen MO, Brill A, Fuchs TA, Savchenko AS, Gallant M, Martinod K, Ten Cate H, Hofstra L, Crijns HJ, Wagner DD, Kietselaer BLJH. Elevated levels of circulating DNA and chromatin are independently associated with severe coronary atherosclerosis and a prothrombotic state. *Arterioscler Thromb Vasc Biol*. 2013;33:2032-2040. doi: 10.1161/ATVBAHA.113.301627.
4. Hornung V, Ablasser A, Charrel-Dennis M, Bauernfeind F, Horvath G, Caffrey DR, Latz E, Fitzgerald KA. AIM2 recognizes cytosolic dsDNA and forms a caspase-1-activating inflammasome with ASC. *Nature*. 2009;458:514-518. doi: 10.1038/nature07725.
5. Hakimi M, Peters A, Becker A, Böckler D, Dihlmann S. Inflammation-related induction of absent in melanoma 2 (AIM2) in vascular cells and atherosclerotic lesions suggests a role in vascular pathogenesis. *J Vasc Surg*. 2014;59:794-803. doi: 10.1016/j.jvs.2013.03.048.

Figure

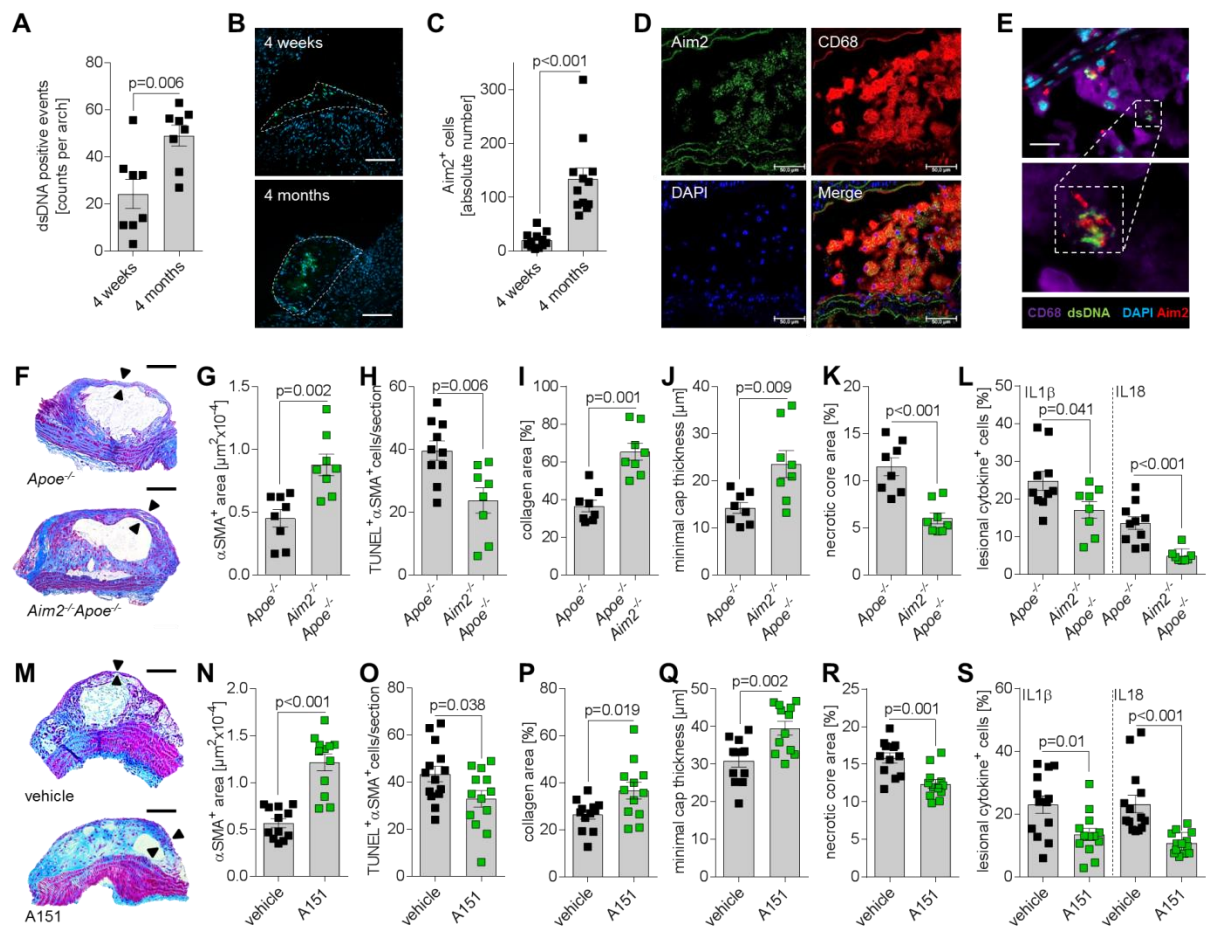


Figure: Neutralization of Aim2 promotes atherosclerotic plaque stabilization.

(A-E) *Apoe*^{-/-} mice were fed a high fat diet for 4 weeks or 4 months. (A) Quantification of dsDNA positive events in aortic arch sections of *Apoe*^{-/-} mice. (B) Representative images showing anti-dsDNA staining (green) and nuclear counterstain (blue). Scale bar, 100 μm . (C) Quantification of Aim2 expression in aortic arch sections. Graph shows the number of Aim2 positive cells from atherosclerotic arch lesions. (D) Confocal microscopy images of representative aortic arch sections from *Apoe*^{-/-} mice after 4 months of high fat diet feeding. Cell nuclei (DAPI, blue), anti-Aim2 (FITC, green), anti-CD68 (Cy5, red). Scale bar, 50 μm . (E) Immunofluorescence aortic arch staining of the outlined region demonstrated colocalization of Aim2 (red), dsDNA (green) in CD68-positive cells (purple), scale bar 10 μm . (F-L) *Apoe*^{-/-} and *Aim2*^{-/-}*Apoe*^{-/-} mice were fed a high fat diet for 4 months. (F) Representative images of Masson's trichrome-stained mouse lesions. Arrows indicate fibrous cap thickness. (G) Enumeration of lesional smooth muscle cells. (H) Quantification of TUNEL⁺ smooth muscle cells. (I) Analysis of lesional collagen content. (J) Assessment of minimal fibrous cap

thickness. **(K)** Quantification of necrotic core area. **(L)** Assessment of lesional IL1 β - and IL18-positive cells. **(M-S)** After 8 weeks high fat diet feeding *ApoE*^{-/-} mice received either PBS or the Aim2 inhibitor A151 (3x/week, i.p.) during another 8 weeks of high fat diet feeding. **(M)** Representative images of Masson's trichrome-stained mouse lesions. Arrows indicate fibrous cap thickness. **(N)** Quantification of lesional smooth muscle cells. **(O)** Enumeration of TUNEL⁺ smooth muscle cells. **(P)** Quantitative assessment of lesional collagen deposition. **(Q)** Measurement of minimal fibrous cap thickness. **(R)** Quantification of necrotic core area. **(S)** Assessment of lesional IL1 β - and IL18-positive cells. All data are presented as mean \pm SEM. Statistical analysis was carried out using unpaired t-test. Individual data points represent one mouse.

Annexin A1 induces a pro-angiogenic macrophage phenotype to promote myocardial repair

Brief title: Annexin A1 promotes myocardial repair

Bartolo Ferraro PhD,^{a,b*} Giovanna Leoni PhD,^{a,b*} Rabea Hinkel DVM,^{b,c,d} Steffen Ormanns MD,^e Nicole Paulin DVM,^{a,b} Almudena Ortega-Gomez PhD,^{a,b} Joana R. Viola PhD,^{a,b} Renske de Jong PhD,^a Dario Bongiovanni MD,^{b,c} Tarik Bozoglu,^c Sanne L. Maas MSc,^{a,b} Michele D'Amico PhD,^f Thorsten Kessler MD,^{b,g} Tanja Zeller PhD,^{h,i} Michael Hristov MD,^a Chris Reutelingsperger PhD,^j Hendrik B. Sager MD,^{b,g} Yvonne Döring, PhD,^{a,b} Matthias Nahrendorf MD,^k Christian Kupatt MD,^{b,c} Oliver Soehnlein MD, PhD.^{a,b,l}

^a Institute for Cardiovascular Prevention (IPEK), LMU Munich, Munich, 80336, Germany

^b DZHK, partner site Munich Heart Alliance, Munich, 80336, Germany

^c Medizinische Klinik I, TU Munich, 81675, Germany

^d Deutsches Primatenzentrum GmbH, Leibniz-Institut für Primatenforschung, Department of Laboratory Animal Science, 37077, Göttingen, Germany

^e Institute of Pathology, Faculty of Medicine, LMU Munich, Munich, 80336, Germany

^f Department of Experimental Medicine, University of Campania, 80138, Italy

^g Department of Cardiology, German Heart Center Munich, Munich, 80636, Germany

^h DZHK, Partner Site Hamburg/Kiel/Lübeck, Hamburg, 20246, Germany

ⁱ Clinic for Cardiology, University Heart Center, Hamburg, 20246, Germany

^j Department of Biochemistry, CARIM, University Maastricht, 6229, the Netherlands

^k Center for Systems Biology, Massachusetts General Hospital, Harvard Medical School, Boston, MA 02114, United States

^l Department of Physiology and Pharmacology (FyFa) & Department of Medicine, Karolinska Institutet, Stockholm, 17177, Sweden

- Data supplement -

Expanded methods section

Histological and immunofluorescence analysis

Hearts were extracted and placed in 4% paraformaldehyde overnight, then transferred to 30% sucrose for 24h and to OCT thereafter. Fixation, tissue processing, antigen retrieval and blocking of nonspecific staining of 4µm sections were performed. Samples were incubated in primary antibody at 4°C overnight. After washing, sections were incubated in the appropriate fluorescent-labeled secondary antibodies followed by counterstaining with DAPI and then mounted in ProLong® Diamond Antifade Mountant (LifeTechnologies, #P36970). The following primary antibodies were used: anti-CD31 (Biolegend, #102502 and Abcam, #ab28364), anti-Endoglin/CD105 (R&D systems, #AF1320), anti- α -smooth muscle actin antibody (Dako, #M0851), anti-Mac2 (Cedarlane, #CL8942AP), anti-Ly6G (eBioscience, #46-9668-82), anti-NG2 (R&D systems, #MAB6689), anti-Troponin I (abcam, #19615), anti-Annexin A1 (ThermoFisher scientific, #71-3400), anti-angiopoietin-1 (R&D Systems, #AF923), anti-FGFb (R&D systems, #AF-233-NA), anti-PDGF (Novus Biological, N#BP1-58279), anti-VEGF-A (Abcam, #ab46154), anti-cleaved caspase-3 (Cell Signaling, #9661), anti-CD68 (eBioscience, #14-0688-82). For Sirius red staining, sections were incubated with 0.1% Sirius red in saturated picric acid for 60min.

Infarct size analysis was performed on transversely sliced sections of the entire heart. TTC staining was used to assess myocardial tissue viability and determine myocardial infarct size. The tissue slices were incubated in 1% TTC solution. Tissues were fixed in 10% PBS-buffered formalin overnight at 2–8°C. TTC-stained tissue slices were photographed and analyzed using ImageJ.

2 photon imaging of the heart

Hearts were permeabilized with 20% horse serum, and 0.5 Triton x-100 at room temperature for 12 hours. Then, samples were incubated with anti-CD31 conjugated to Alexa Fluor 488 (ThermoFisher, 1:50) overnight at 4°C. The tissue was imaged in z stacks, using a Leica SP5 two-photon laser scanning microscope with a pre-chirped and pulsed Ti:Sapphire Laser (Spectra Physics MaiTai Deepsee) tuned at 750nm and a 20×NA1.00 (Leica) water dipping objective. Image acquisition and processing was performed using LasX software (Leica).

Myocardial infarction autopsy tissue

The use of human tissue samples was approved by the local ethics committee (18-554 UE). Tissue blocks of formalin fixed paraffin embedded (FFPE) myocardial tissue with histologically confirmed acute myocardial infarction obtained during routine clinical autopsies between 2014 and 2017 were retrieved from the archives of the Institute of Pathology. Only patients who deceased from an acute or relapsed acute myocardial infarction were included. Patients suffering from inflammatory conditions such as sepsis, malignant neoplastic diseases or other severe concomitant conditions according to their clinical and pathological records were excluded from the study. Tissue blocks containing sufficient vital myocardial tissue next to areas of acute infarction were selected and the diagnosis of myocardial infarction confirmed by an experienced pathologist on HE stained sections. Subsequently, 4 µm thick whole mount tissue sections were prepared for immunofluorescence staining. Sections were deparaffinized, rehydrated, antigen retrieval and blocking of non-specific antibody binding were performed. Samples were incubated in primary antibody at 4°C overnight. The following primary antibodies were used: PE conjugated anti-human CD31 (eBioscience, #12-0319-73), FITC conjugated anti-human CD68 (eBioscience, #11-0689-42), anti-Annexin A1 (ThermoFisher scientific, #71-3400) and anti-VEGF-A (Abcam, #ab46154). After washing, sections were incubated in the appropriate fluorescent-labeled secondary

antibodies, when needed, followed by counterstaining with DAPI and then mounted in ProLong® Diamond Antifade Mountant (LifeTechnologies, #P36970).

Flow cytometry

The cardiac tissues were digested in a buffer containing collagenase (450U/ml, Sigma-Aldrich, #C5138), hyaluronidase type I-s (60U/ml Sigma-Aldrich, #H3506), and DNase (60U/ml, Sigma-Aldrich, #AMPD1) at 37°C for 1h. Single cell suspensions, derived from myocardial tissue or blood, were incubated with antibodies to CD45 (eBioscience, #47-0451-82), CD11b (eBioscience, #25-0112-82), Ly6G (eBioscience, #145931), F4/80 (eBioscience, #17-4801-82), Ly6C (BioLegend, #128018), MHCII (BioLegend, #107618), CD31 (eBioscience, #48-0311-82), and DDR2 (Santa Cruz Biotechnology, #sc-7555) and samples were acquired using a BD FACSCanto™ II.

Conditioned medium

After FACS sorting (BD FACSAria III) cardiac macrophages, endothelial cells and fibroblasts were seeded on a 48 well plate, and stimulated for 24h with PBS or hrAnxA1 (100nM). The conditioned medium of each cardiac cell population was collected and analyzed for the release of pro-angiogenic factors and analyzed for its functional effects on endothelial cell activity. When indicated, cardiac macrophages were cultured in hypoxic conditions (1% oxygen, 5% CO₂).

5µl of supernatant were spotted onto nitrocellulose membrane and were allowed to dry at room temperature. The membrane was incubated in blocking solution before overnight incubation with the primary antibody. The membrane was rinsed 5 times with TBST before incubation with the HRP-conjugated secondary antibody. Signals were detected by chemiluminescence. The signal intensity of each dot was analyzed using Image Lab™ Software.

Endothelial cell assays

SV40-transformed mouse endothelial cells (SVECs) were grown in high-glucose (4.5g/l) DMEM. In wound healing assays, SVECs were cultured to confluence in a 48 wells plate. On the day of the assay a sterile 200µl pipet tip was used to scratch the monolayer. A picture per each wound was taken at time 0 and after 16h. Endothelial cells were incubated with conditioned media derived from cultured cardiac macrophages post-MI. For the calculation of the results, the surface area of the defined initial wound area (time 0) and the surface area of the migrated cells in to the wound area (time 16h) were measured. Endothelial cell viability was assessed by trypan blue staining. To study tube formation, 96-well plates were filled with 70µl Matrigel (Corning, #354230) and SVECs were seeded on top of the gel. Subsequently, endothelial cells were incubated with conditioned media derived from cultured cardiac macrophages post-MI. After 24h time the network structures were stained with CellMask™ Orange Plasma membrane Stain (Life Technologies, #C10045) and images were taken and quantified. When indicated, supernatants were supplemented with a VEGF164 neutralizing antibody (R&D systems, #AF-493-NA) at a concentration of 10 ng/ml.

Western blot analysis

To evaluate pVEGFR2, pFAK and pAKT expression, proteins were extracted from a monolayer of endothelial cells after treatment with conditioned media derived from cardiac macrophages obtained from *AnxAI*^{-/-} or WT mice. 10µg of protein extract was separated by SDS-PAGE and probed with the following primary antibodies: anti-phospho-VEGF receptor 2 (Cell Signaling, #2478), anti-phospho-FAK (Thermo Fisher, #700255), anti-phospho-AKT (Cell Signaling, #4060), and anti-β-actin (Cell Signaling, #4970). Western blotting bands were visualized with the clarity western ECL substrate (BioRad, #170-5060) and the signal

intensity was analyzed using Image Lab™ Software. Results were normalized using β -actin as housekeeper and expressed as arbitrary units (AU).

Annexin A1 recombinant protein purification

cDNA of human AnxA1 carrying a cleavable N-terminal poly-His tag was expressed in *E. coli*. Recombinant protein was purified on IMAC (GE Healthcare), and the poly-His tag was subsequently removed. Purity of recombinant AnxA1 was confirmed by SDS-PAGE and the 4800 MALDI-TOF/TOF (Applied Biosystems), revealing a 38.6 kDa protein that was >95% pure. Endotoxin was determined with the Endosafe-PTS (FDA-licensed LAL cartridge from Charles-River) according to the manufacturer's protocol. hrAnxA1 contained < 0.2 units endotoxin per mg hrAnxA1.

Pig experimentation

Fourteen days before ischemia/reperfusion injury, the myocardium was transduced with human AnxA1 by selective pressure regulated retroinfusion of 5×10^{12} rAAV.AnxA1 particles into the anterior ventricular vein, which anatomically drains the LAD-perfused myocardium (1). The vector was designed to express the human Annexin 1 under the control of the constitutive cytomegalovirus (CMV) enhancer/promoter. Recombinant AAV genomes containing AAV2 inverted terminal repeats (ITRs) were with a cis-plasmid containing the Annexin 1 transgene, an adenovirus helper plasmid, and a chimeric trans-plasmid containing the AAV2 rep gene fused to the capsid gene of the AAV 9 serotype were used. We generated this by opening the pAAV.CMV.LacZ vector backbone NotI and HindIII, and excising the insert by EAGI and BamHI. Fragments were blunted and ligated. pAAV.CMV.LacZ vector was also used to produce of negative control virus. Specific cardiomyocytic transduction is achieved by selectivity of AAV9 capsid and permissiveness of the CMV promoter (2). RNA fluorescence in situ hybridization (FISH) on pig heart tissues was used to confirm expression

of human Annexin A1. RNA FISH assay was performed using the Affymetrix protocol (ViewRNA Cell Plus Assay, Affymetrix) with some modifications. Briefly, freshly cut pig heart specimens were incubated with custom probe oligonucleotides specific for human Annexin A1 and pig Beta-2 microglobulin designed and synthesized by Affymetrix as Type 1 (Catalog number VA1-3000191) and 6 (Catalog number VF6-20733), respectively, following the manufacturer instructions. At the end of the hybridization, sections were counterstained with DAPI and images were taken with a fluorescent microscope at 40x magnification. In all pig experimentation, we used an AAV2/9. For this serotype, we have found favorable transduction in porcine (German landrace) hearts *in vivo* (3). Pigs were anesthetized with intramuscular injection of azaperon, ketamine and atropine and maintained *via* i.v. application of midazolam and fentanyl. Subsequently, pigs underwent endotracheal intubation and anesthesia was maintained by infusion of propofol and fentanyl. After introduction of sheath into the common carotid artery a guiding catheter and transluminal coronary angioplasty balloon catheter were placed in the LAD and inflated with 6 atm for 60 min. Correct localization of the coronary occlusion and patency of the first diagonal branch were ensured by injection of contrast agent *via* the guiding catheter. In all groups, the PTCA balloon was deflated after 60min of ischemia; the onset of reperfusion was documented angiographically. After 7d of reperfusion, hemodynamic measurements were performed and the pigs were sacrificed for further analysis of the infarct size as described (1).

Statistics

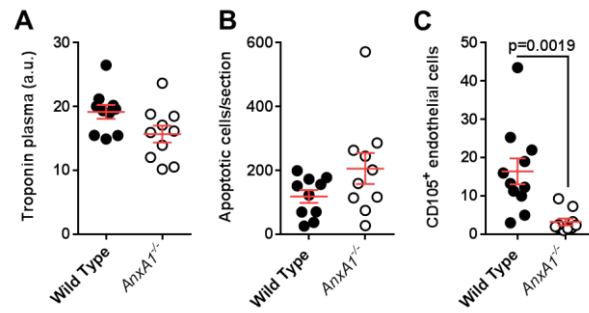
All data are expressed as mean \pm SEM and statistical analysis was performed with Prism Software. For each graph normality was assessed by using the Shapiro-Wilk normality test. Thereafter, the unpaired Student *t*-test, one-way analysis of variance (ANOVA) or nonparametric Mann-Whitney test or Kruskal-Wallis test were used as appropriate. For parallel repeated measures studies 2-way ANOVA followed by Bonferroni post-hoc test was

used to determine the significance for individual time points. $P < 0.05$ was considered significant.

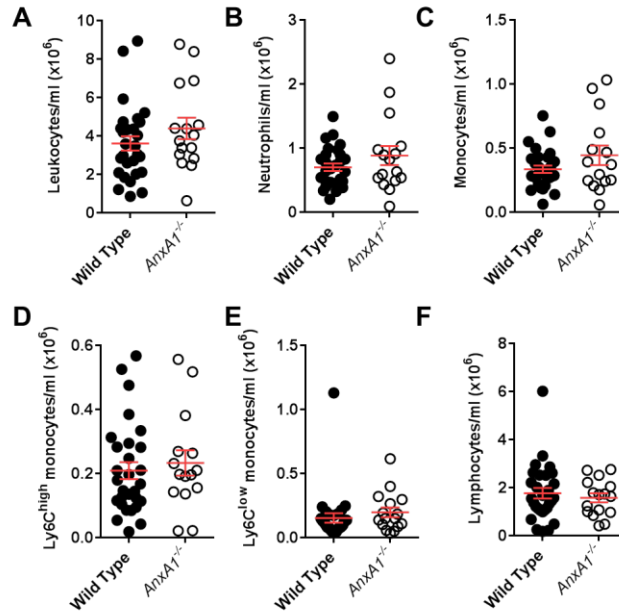
Supplementary References:

1. Hinkel R, Lange P, Petersen B, et al. Heme Oxygenase-1 Gene Therapy Provides Cardioprotection Via Control of Post-Ischemic Inflammation: An Experimental Study in a Pre-Clinical Pig Model. *J Am Coll Cardiol* 2015;66:154-65.
2. Bish LT, Morine K, Sleeper MM, et al. Adeno-associated virus (AAV) serotype 9 provides global cardiac gene transfer superior to AAV1, AAV6, AAV7, and AAV8 in the mouse and rat. *Hum Gene Ther.* 2008;19:1359-68.
3. Postrach J, Schmidt M, Thormann M, et al. Adeno-associated viral vector 2.9 thymosin β 4 application attenuates rejection after heart transplantation: results of a preclinical study in the pig. *Transplantation* 2014;98:835-43.

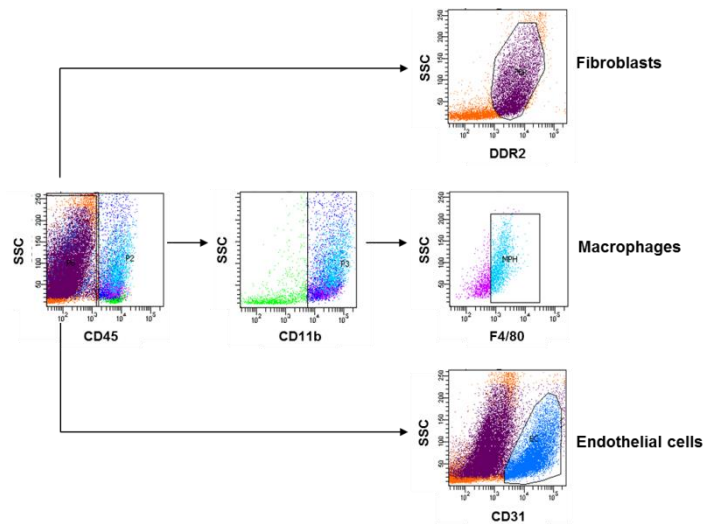
Supplemental figures



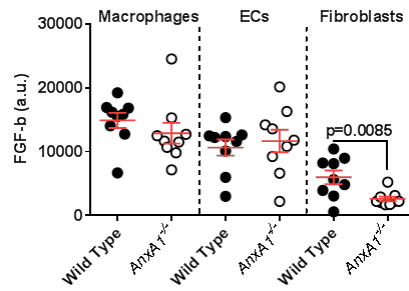
Online Figure 1: Lack of Annexin A1 does not impact on plasma troponin levels and apoptotic cell accumulation in the heart but on neangiogenesis. Myocardial infarction was induced in WT and *AnxAI*^{-/-} mice. Plasma Troponin I (A) and myocardial apoptotic cells (B) 6 days after induction of MI were quantified. (C) Quantification of CD105⁺CD31⁺ cells in heart sections. Unpaired t-test. Values are mean±SEM. Each dot represents one mouse.



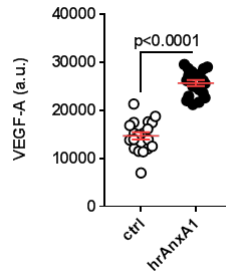
Online Figure 2: Annexin A1 deficiency does not affect the number of circulating leukocytes. FACS quantification of (A) total leukocytes, (B) neutrophils, (C) monocytes, (D) Ly6C^{high} monocytes, (E) Ly6C^{low} monocytes and (F) lymphocytes circulating in the blood of WT and *AnxA1*^{-/-} mice after 6 days of MI, (A, B, D, E, F) Mann Whitney test, (C) unpaired t-test. All values are mean \pm SEM. Each dot represents one mouse.



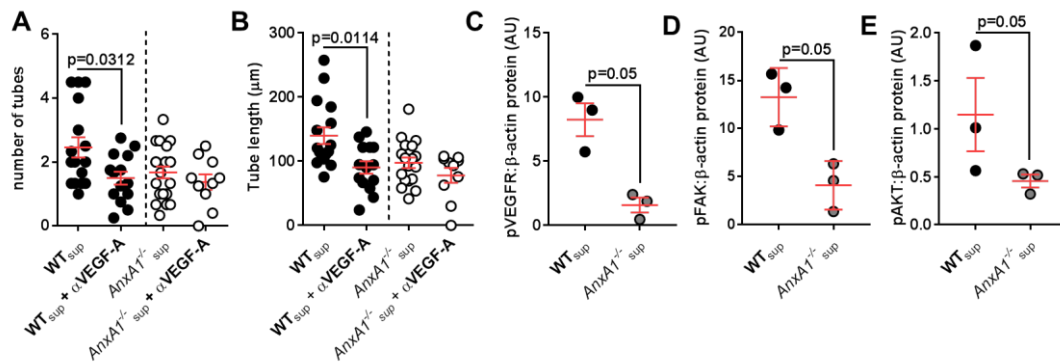
Online Figure 3: Gating strategy to sort cardiac macrophages, fibroblasts and endothelial cells from heart homogenates. Macrophages were identified as CD45⁺CD11b⁺F4/80⁺; fibroblasts as CD45⁻DDR2⁺ and endothelial cells as CD45⁻CD31⁺.



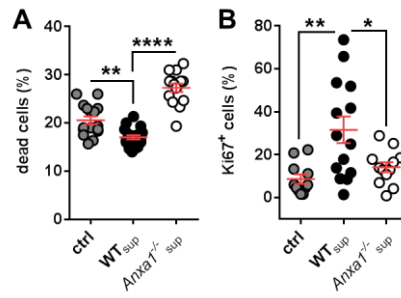
Online Figure 4: Lack of Annexin A1 reduces FGF-b release from cardiac fibroblasts. Indicated populations were FACS-sorted from WT and *AnxA1*^{-/-} mice heart homogenates 6 days post-MI. FGF-b was assessed by dot blot analyses. Mann-Whitney test for macrophages and fibroblasts, unpaired t- test for endothelial cells. Values are mean±SEM. Each dot represents one mouse.



Online Figure 5: Annexin A1 induces VEGF-A release from macrophages under hypoxia. Quantification of VEGF-A released from WT cardiac macrophages isolated 6d post MI treated with PBS (ctrl) or AnxA1 (hrAnxA1, 100 nM). Macrophages were cultured under hypoxia conditions. Values are mean \pm SEM. Data were analyzed with unpaired t-test. Each dot represents the supernatant generated in one well.

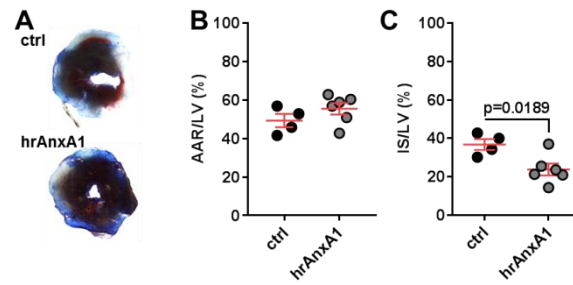


Online Figure 6: Annexin A1 promotes endothelial activation and tube formation through VEGF-A. (A/B) Endothelial cells were grown in basement membrane matrix and (A) tube number and (B) length were evaluated after treatment with conditioned medium derived from cardiac WT macrophages (WT_{sup}) or in presence of conditioned media derived from *AnxA1*^{-/-} macrophages (*AnxA1*^{-/-}_{sup}) 6d post MI. Where indicated a VEGF-A neutralizing antibody (10 ng/ml) was present. Values are mean \pm SEM. Data were analyzed with Mann-Whitney test. Each dot represents one well, in each well several fields of view were observed and averaged. (C-E) Endothelial cells were treated with conditioned medium derived from cardiac WT macrophages (WT_{sup}) or in presence of conditioned media derived from *AnxA1*^{-/-} macrophages (*AnxA1*^{-/-}_{sup}) 6d post MI. Protein was extracted and the phosphorylation of VEGFR2 (C), FAK (D), and AKT (E) was assessed by western blot. Data are normalized to β -actin. Values are mean \pm SEM. Data were analyzed with Mann-Whitney test. Each dot represents one mouse.

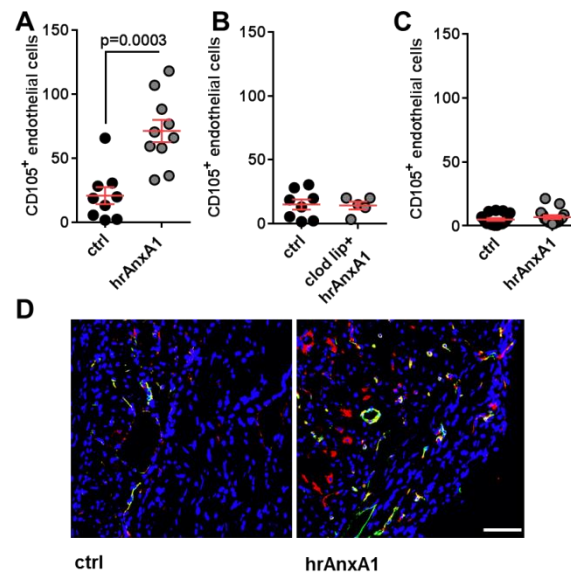


Online Figure 7: Annexin A1 stimulates endothelial cell proliferation and survival.

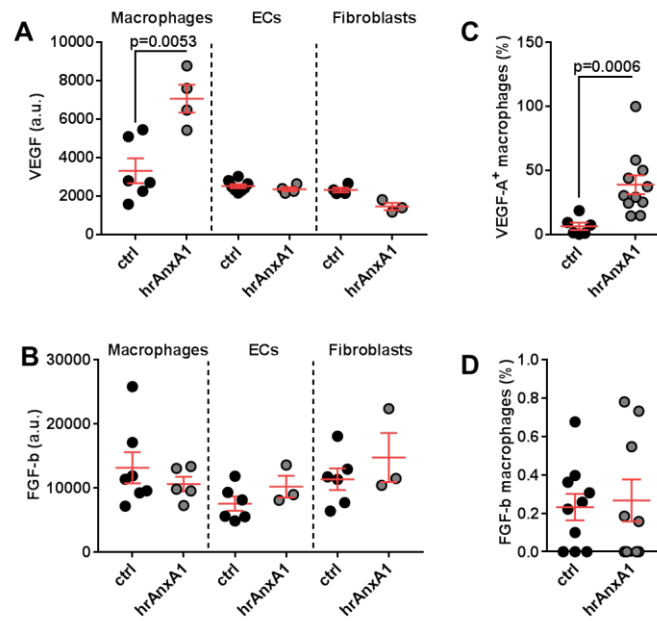
Quantification of death (A) and proliferation (B) in endothelial cell monolayers in the presence of conditioned medium derived from cardiac WT macrophages (WT_{sup}) or *AnxA1*^{-/-} macrophages (*AnxA1*^{-/-}_{sup}). P-values were calculated using one-way ANOVA. Values are mean±SEM. Each dot represents one well, in each well several fields of view were observed and averaged.



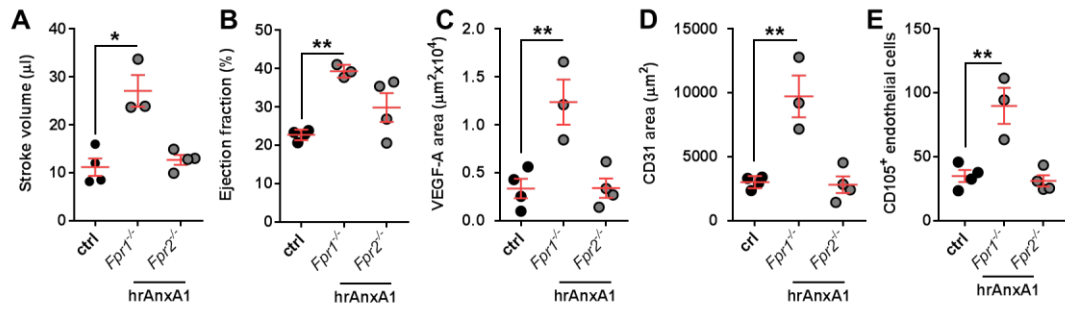
Online Figure 8: Annexin A1 treatment reduces infarct size. WT mice were treated with PBS or hrAnxA1 (10 μ g/d/mouse, i.p.). (A) Representative images after Evans Blue injection and subsequent TTC staining. Displayed are area at risk (B) and infarct size relative to left ventricle sizes (C). Values are mean \pm SEM. Data were analyzed with unpaired t-test. Each dot represents one mouse.



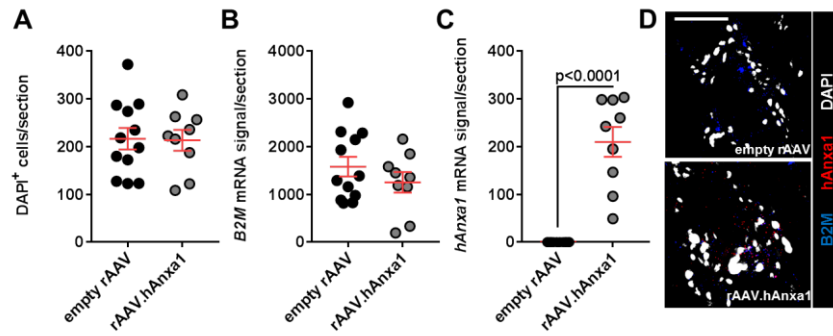
Online Figure 9: Annexin A1 treatment improves neoangiogenesis within the infarct area. Neoangiogenesis was monitored using an antibody against endoglin (CD105), a cell-surface glycoprotein highly expressed on proliferating endothelial cells. **(A)** Quantification of endoglin immunostaining in mice treated with human recombinant Annexin A1 treatment (hrAnxA1) compared to the control group (ctrl), unpaired t-test. **(B)** Neoangiogenesis was assessed after macrophage depletion using clodronate loaded liposomes and **(C)** after bone marrow transplantation, to selectively deplete VEGF-A in macrophages. P-values were calculated using Mann-Whitney test. Values are mean \pm SEM. **(D)** Representative images showing the new blood vessels within the infarct area of hrAnxA1 treated mice compared to the control group (PBS treated) after 6 days of permanent ligation of the LAD. The new blood vessels are stained using the CD31 (green) and CD105 (red) as endothelial cells markers and DAPI (blue) to counterstain the nuclei. Scale bar, 50 μ m. Each dot represents one mouse.



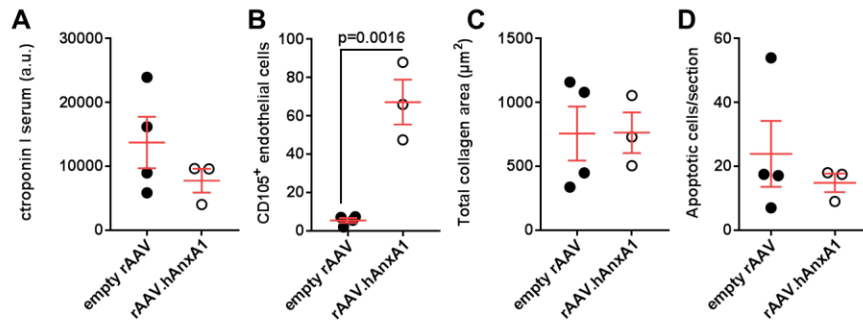
Online Figure 10: Annexin A1 delivery stimulates VEGF-A but not FGF-b release from macrophages. Assessment of (A) VEGF-A and (B) FGF-b released in the medium derived from cardiac macrophages, endothelial cells (EC) and fibroblasts 6 days post MI after PBS (ctrl) or hrAnxA1 treatment, unpaired t-test. (C) Percentage of cardiac macrophages expressing VEGF-A and (D) FGF-b vs. total amount of cardiac macrophages in the myocardium after 6 days MI, Mann-Whitney test. Values are mean \pm SEM. Each dot represents one well, in each well several fields of view were observed and averaged.



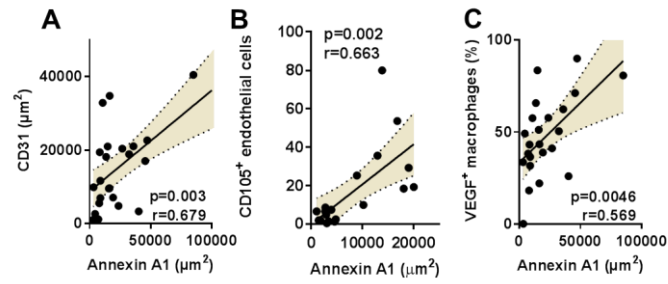
Online Figure 11: Annexin A1 regulates cardiac repair via FPR2. All mice underwent LAD ligation and analyses were performed 6 days after. WT mice were treated with PBS (ctrl), while *Fpr1*^{-/-} and *Fpr2*^{-/-} mice received hrAnxA1 (10 $\mu\text{g}/\text{d}/\text{mouse}$, i.p.) and cardiac function and angiogenesis were assessed. **(A)** Stroke volume, Kruskal-Wallis test. **(B)** Ejection fraction, one-way Anova. **(C)** Quantification of myocardial VEGF-A expression, one-way Anova. **(D)** Assessment of myocardial CD31 immunostaining, one-way Anova. **(E)** Enumeration of newly formed CD105⁺CD31⁺ endothelial cells, one-way Anova



Online Figure 12: Overexpression of human AnxA1 in pig hearts. Pigs were treated with an empty adenovirus (empty rAAV) or and with an AAV promoting hAnxa1 expression (rAAV.hAnxa1) two weeks prior to ischemia-reperfusion injury. Hearts were obtained 7 days post reperfusion and sections of the area at risk were incubated with probes specific for beta2-microglobulin (B2M, B) and human AnxA1 (hAnxa1, C) and counterstained with DAPI (A). Representative images are shown in D. Scale bar 50 μm . Each dot represents one section, quantified were three sections per pig. Unpaired t-test.



Online Figure 13: Overexpression of Annexin A1 does not impact on serum Troponin levels, cardiac collagen deposition, and cardiac cell apoptosis. Pigs were treated with an empty adenovirus (empty rAAV) or and with an AAV promoting AnxA1 expression (rAAV.AnxA1) two weeks prior to ischemia-reperfusion injury. Displayed are serum troponin (A), CD105⁺CD31⁺ endothelial cells (B), cardiac collagen (C), and number of cardiac apoptotic cells (D). All values are mean±SEM. Each dot represents one pig.



Online Figure 14: Annexin A1 correlates with parameters of angiogenesis in human hearts. Human heart sections derived from patients with acute myocardial infarct were stained with antibodies to Annexin A1, CD31, VEGF-A, and CD68. Pearson correlations were calculated for Annexin A1 and CD31 (A), Annexin A1 and CD105⁺CD31⁺ cells (B), as well as for Annexin A1 and VEGF-A within macrophages (C). Dotted lines indicate 95% confidence interval. Each dot represents one patient.

Video S1: Echocardiography in WT mice treated with PBS 6 days post MI. WT mice were treated with PBS and cardiac function was assessed by echocardiography. Displayed is a left parasternal long-axis view in B-mode.

Video S2: Echocardiography in WT mice treated with hrAnxA1 6 days post MI. WT mice were treated with hrAnxA1 (10 μ g/d/mouse, i.p.) and cardiac function was assessed by echocardiography. Displayed is a left parasternal long-axis view in B-mode.